Observation of a non-equilibrium superradiant phase transition in free space

Giovanni Ferioli, Antoine Glicenstein, Igor Ferrier-Barbut, Antoine Browaeys

Observation of a non-equilibrium superradiant phase transition in free space

Giovanni Ferioli,[1,*] Antoine Glicenstein,[1] Igor Ferrier-Barbut,[1] and Antoine Browaeys[1]

[1] *Université Paris-Saclay, Institut d'Optique Graduate School, CNRS, Laboratoire Charles Fabry, 91127, Palaiseau, France*

We observe a non-equilibrium phase transition in a driven dissipative quantum system consisting of an pencil-shape cloud of up to $N \approx 2000$ laser-cooled atoms in free space, optically excited along its main axis. We find that our data are well reproduced by the Driven Dicke model, which assumes a sub-wavelength sample volume, by simply using an effective atom number. By measuring the excited state population of the atoms and the light emitted in the superradiant mode, we characterize the dynamics of the system and its steady-state properties. In particular, we observe the characteristic N^2 scaling of the photon emission rate in the superradiant phase, thus demonstrating steady-state superradiance in free space. Finally, we observe a modification of the statistics of the superradiant light as we cross the phase transition.

Systems of interacting quantum particles at equilibrium exhibit collective phenomena such as the existence of phases and transitions between them. These phases result from an interplay between interactions and the action of external parameters. Many efforts are currently under way, in particular in a quantum simulation approach, to understand equilibrium properties of quantum many-body systems [1]. Recently, a new class of systems has emerged where dissipation, external drive and interactions compete and give rise to non-equilibrium phases that would not exist without the drive (e.g. [2–5]). In such systems, phase transitions could occur without the breaking of any symmetry, but with a local order parameter, in stark contrast with both the Landau theory of phase transitions at equilibrium and the case of topological transitions [6]. One of the simplest driven-dissipative quantum systems consists of an ensemble of two-level atoms, enclosed in a volume smaller that the wavelength of the atomic transition cubed, as described by Dicke [7], but now driven by a classical light field [6, 8–12]. In this so-called driven Dicke model (DDM), the competition between collective coupling of the atoms to the driving field and their cooperative decay was predicted to lead to a transition between a phase where all the atomic dipoles are phase-locked forming a collective dipole coherently driven by the light, and a phase governed by superradiant spontaneous emission [6]. This model is also expected to exhibit a new type of time crystals [13]. Besides its fundamental interest, steady-state superradiance is used in cavity systems to generate superradiant lasers [14–18], a novel kind of metrologically stable laser sources. Finding cavity-free configurations sustaining steady-state superradiance could simplify experiments and be of interest in metrology.

A key feature of the DDM is the identical (cooperative) coupling of all the atoms to the electromagnetic field, a fact automatically ensured in sub-wavelength samples. However, confining an ensemble of emitters in a sub-wavelength volume is experimentally very challenging in the optical regime. For extended ensembles, the condition of cooperative coupling to the field has thus been realized by placing the emitters in a cavity where they share the same electromagnetic mode [19]. Superradiant phase transition [20, 21] and lasing has been observed in this system. Here instead, we realize the DDM in *free space*, using a pencil-shape cloud of cold atoms, optically excited along its main axis. By measuring both the atomic and photonic degrees of freedom, we observe the transition between the two non-equilibrium phases predicted by the model.

The DDM describes an ensemble of N two-level atoms (states $|g\rangle$ and $|e\rangle$) as a collective spin $\hat{S}^{\pm} = \sum_{i=1}^{N} \hat{\sigma}_i^{\pm}$ (here $\hat{\sigma}_i^{-} = |e_i\rangle\langle g_i| = (\hat{\sigma}_i^{+})^{\dagger}$)[22]. The indiscernability of the atoms with respect to the field restricts the accessible states to the permutationally symmetric ones, $|S = N/2, m = -S, ..., S\rangle$, which form a ladder (see Fig.1a). The Hamiltonian describing the interaction of this collective spin with a classical light field, resonant with the single-atom transition, is $\hat{H}_{\mathrm{L}} = (\hbar\Omega/2)(\hat{S}^{+} + \hat{S}^{-})$, with Ω the Rabi frequency. The dynamics of the collective spin is governed by the equation:

$$\frac{d\rho}{dt} = -\frac{i}{\hbar}[\hat{H}_{\mathrm{L}}, \rho] + \frac{\Gamma}{2}(2\hat{S}^{-}\rho\hat{S}^{+} - \hat{S}^{+}\hat{S}^{-}\rho - \rho\hat{S}^{+}\hat{S}^{-}) \,, \quad (1)$$

where the last term describes the collective spontaneous emission (here Γ is the single-atom decay rate from $|e\rangle$). In steady-state, this model supports two non-equilibrium phases, depending on the ratio between the drive and the collective dissipation $\beta = 2\Omega/(N\Gamma)$[6, 22]. For $\beta < 1$, the atomic dipoles phase-lock and the ensemble develops a collective dipole $\langle \hat{S}^{-} \rangle_{\mathrm{st}} = -i\Omega/\Gamma$, as represented in Fig. 1(b). As β increases, so does the amplitude of the dipole until it reaches its largest value $N/2$ for $\beta = 1$. Conversely, the total magnetization $\langle \hat{S}_z \rangle_{\mathrm{st}}$ decreases to 0. For $\beta \gg 1$, all the states of the ladder are equally populated (see Fig. 1a), the collective dipole vanishes and superradiance dominates with the characteristic N^2 scaling of the photon emission rate. We will refer to the $\beta < 1$-phase as magnetized and the $\beta > 1$-one as superradiant. In the limit $N \to \infty$, the value $\beta = 1$ corresponds to the critical point of a second order phase-transition. These are the two phases that we observe and characterize here.

Our experiment (see Fig. 1c) [23] relies on a cloud of up to $\simeq 2000$ laser-cooled ^{87}Rb atoms placed in a dipole trap. We isolate the two states $|g\rangle = |5S_{1/2}, F = 2, m_F = 2\rangle$ and $|e\rangle = |5P_{3/2}, F = 3, m_F = 3\rangle$ of the D2 transition ($\lambda = 2\pi/k = 780\,\mathrm{nm}$, linewidth $\Gamma \simeq 2\pi \times 6\,\mathrm{MHz}$) using a 96 G-magnetic

* giovanni.ferioli@institutoptique.fr

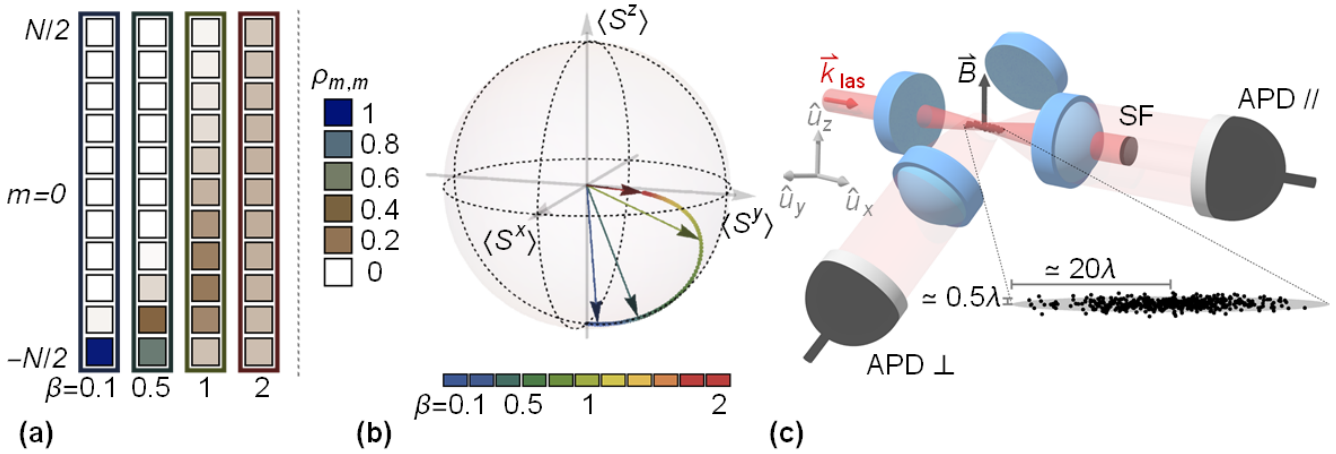

FIG. 1. **Non-equilibrium phases in the Driven Dicke Model.** (a) Populations of the $N+1$ states in the Dicke ladder ($N=10$), corresponding to the vectors reported in (b). (b) Bloch-sphere representation of the collective spin predicted by the steady-state DDM, for different values of β. The collective dipole is $\langle\hat{S}^-\rangle = -i\langle\hat{S}y\rangle$. (c) Experimental setup. A pencil-shape cloud of laser-cooled ^{87}Rb atoms is prepared in a dipole trap (not shown), placed between four high-numerical aperture lenses. A resonant laser beam propagates along the main axis of the cloud ($1/e^2$-radius of 5 μm). Its linear polarization is perpendicular to the magnetic field $\vec{B}$, so that only the σ^+ component of the light drives the atoms. The emitted light is collected in two different directions by two fiber-coupled avalanche photodiodes, APD// and APD$\perp$, operating in single photon counting modes. APD$\perp$ gives access to the atomic excited state population (magnetization). A spatial filtering (SF) separates the laser light from the one emitted axially by the cloud, so that APD// measures the rate of superradiant light emission $\gamma_{SR}(t)$.

field. The ensemble has axial and radial sizes $\ell_{ax} = 20-25\lambda$ and 0.5λ. The mean distance between atoms in the cloud is $r \sim 3/k$, so that the coherent dipole interactions can be neglected, especially considering the large driving intensity used in the experiment [22, 24]. As shown below, this pencil-shape ensemble of two-level atoms driven along its main axis realizes the DDM, valid for sub-wavelength sample, by simply considering an effective atom number $\tilde{N} = N\mu$. The parameter $\mu \sim \Delta\Theta/(4\pi)$ characterizes the coupling of the extended cloud to its diffraction mode extending over a solid angle $\Delta\Theta$ [22, 25–27], and $\tilde{N}$ is equivalent to the N-atom cooperativity in cavity systems [19]. Here $\mu \sim \lambda/(2\pi\ell_{ax})$, allowing us to reach $\tilde{N} \sim 10$, a value sufficiently large to observe the crossover between the two non-equilibrium phases of the DDM. After optically pumping the atoms in $|g\rangle$ and switching off the trap for ~ 500 ns, we excite the cloud with 150 ns-long pulses of a resonant laser beam propagating along its main axis. We repeat this procedure 30 times on the same cloud and average over ~ 2000 clouds. We measure the number of emitted photons in two orthogonal directions with avalanche photodiodes (APDs). The first one (APD$\perp$), radially aligned, is sensitive to the excited state population $n_e(t)$, related to the magnetization $s_z(t) = 2n_e(t) - 1$. This quantity acts as an order parameter for the system. The second one (APD//) measures the photon emission rate in the superradiant mode $\gamma_{SR}(t) = \Gamma\langle\hat{S}^+\hat{S}^-\rangle$ [26, 28].

We start by investigating the dynamics of the magnetization during the application of a laser excitation pulse. First, we fix the Rabi frequency of the laser driving to $\Omega = 4.5\Gamma$ and vary N. Examples of experimental curves for different N are reported in Fig. 2 (a). For low N, the dynamics is well described by the solution of the two-level optical Bloch equations (OBEs), indicating independent atom behavior. As

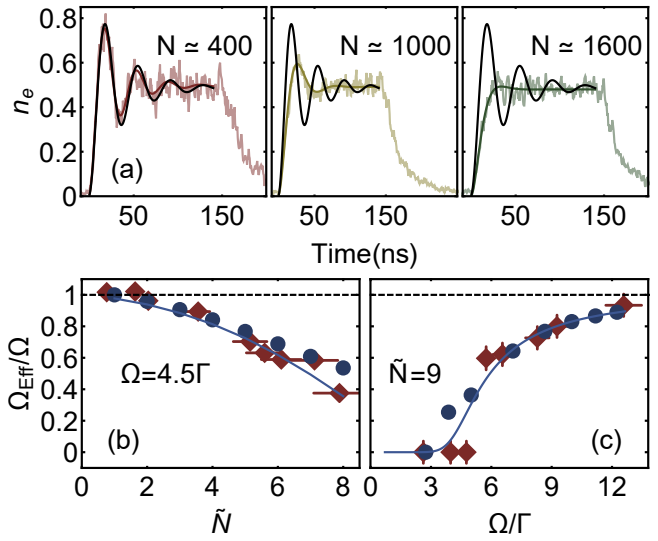

FIG. 2. **Collective dynamics during excitation.** (a) Excited state population $n_e(t)$ during the laser pulse measured with APD$\perp$ (temporal bins: 1 ns), for different N. Black line: solution of OBEs. Colored line: fit using the analytical solution of the OBEs. (b,c) Colored diamonds: experimental values Ω_{Eff} as a function of $\tilde{N} = N\mu$ (b) and of Ω (c). Error bars on Ω_{Eff} from the fit. Uncertainties on $\tilde{N}$ and Ω: 10% shot-to-shot fluctuations. Blue dots: prediction from the solution of the time-dependent DDM fitted as in the experiment. Continuous blue lines: Ω_{Eff} from the steady state of the DDM.

N increases, we observe a reduction of the frequency and amplitude of the oscillations, until they vanish for the largest N. We fit each curve by the analytical solution of OBEs [29], with an effective Rabi frequency Ω_{Eff} and the decay rate

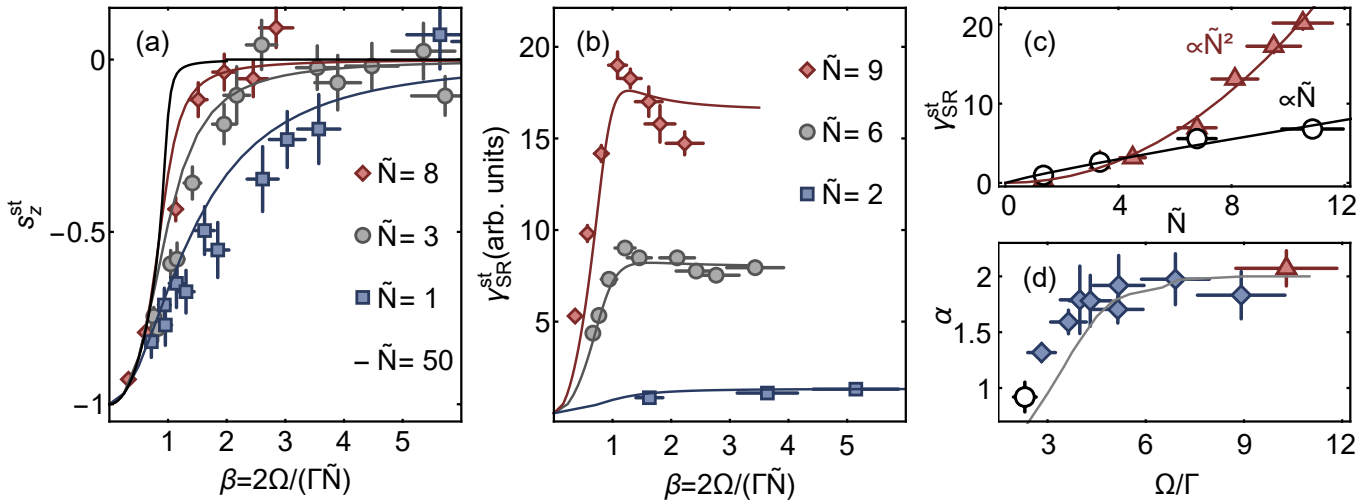

FIG. 3. **Onset of the superradiant phase.** (a,b) Experimental steady-state values of s_z and γ_{SR} as a function of β, for different atom numbers $\tilde{N}$. Lines: predictions of the DDM. (c): examples of the dependence $\gamma_{SR} \propto \tilde{N}^{\alpha}$ in the weak (black empty-circles, $\Omega \simeq 2.5\,\Gamma$) and strong (red triangles, $\Omega \simeq 10\Gamma$) driving regimes. (d) Exponent α of the fit. Grey line: prediction of the DDM. Error bars on s_z^{st} and γ_{SR}^{st}: standard error on the mean. For α: error from the fit.

as free parameters. Figure 2(b) reports the fitted values of Ω_{Eff}, which decrease as N increases. Second, we perform the complementary experiment where we fix $\tilde{N} \simeq 9$ and vary Ω. We observe oscillations of n_e only above a critical driving strength Ω_c, and Ω_{Eff} becomes comparable to Ω only in the strongly driven regime ($\Omega > 10\Gamma$).

Our observations can be explained in the framework of the DDM. When driven by the laser, the ensemble develops a collective dipole $\langle\hat{S}^-\rangle$, which in turn radiates a field whose amplitude inside the cloud is $\langle\hat{E}_{Sc}\rangle = -i\hbar\Gamma\langle\hat{S}^-\rangle/d$ (d is the dipole matrix element of the $e-g$ transition) [11, 12, 22]. The field E_{Eff} in the cloud results from the superposition of the laser field $E_L = \hbar\Omega/d$ and of $\langle E_{Sc}\rangle$, yielding an effective Rabi frequency $\Omega_{Eff} = dE_{Eff}/\hbar = \Omega - i\Gamma\langle\hat{S}^-\rangle$. For a resonant excitation, $\langle\hat{S}^-\rangle$ is purely imaginary so that $|\Omega_{Eff}| \leq \Omega$: the collective dipole gives rise to a π-shifted field which screens the laser field. Qualitatively, the screening increases with the amplitude of the collective dipole, hence with N. To compare quantitatively the data to the DDM, we solve numerically Eq. (1) to get $n_e(t)$, and fit the solution with the same functional form as for the data. The only free parameter in the simulation is $\mu = \tilde{N}/N$. We find a good agreement between the theoretical prediction and the experimental results for $\mu \simeq 0.005$, as shown in Fig. 2(b,c). Considering the errors on the determination of the cloud sizes and atom numbers, this value is consistent with the inferred one (see [22]).

We also calculate the *steady-state* solution of Eq. (1) to extract $\langle\hat{S}^-\rangle$ and thus Ω_{Eff}, using the value of μ obtained above. As visible in Fig. 2(b,c), the steady-state values of Ω_{Eff} matches the ones extracted from the dynamics. This fact indicates that, for $\beta = 2\Omega/\Gamma\tilde{N} < 1$, the collective coherence giving rise to the screening is established inside the cloud in a timescale ($\sim 1/\tilde{N}\Gamma$) faster than the driving period $1/\Omega$. Thus, $\Omega_{Eff} \approx \Omega - i\Gamma\langle\hat{S}^-\rangle_{st}$. The existence of the threshold in Ω observed in Fig. 2(b,c) can now be understood: for a given $\tilde{N}$, and for $\beta \leq 1$ (magnetized phase), $\langle\hat{S}^-\rangle_{st} = i\Omega/\Gamma$, so that $\Omega_{Eff} \approx 0$ up to a critical driving strength $\Omega_c/\Gamma = \tilde{N}/2$ where the dipole reaches its largest amplitude. For $\Omega \gg \Omega_c$ ($\beta \gg 1$), the system is saturated, $\langle\hat{S}^-\rangle_{st}$ vanishes, and $\Omega_{Eff} \simeq \Omega$. Conversely, for a fixed value of $\Omega/\Gamma > 1$, increasing $\tilde{N}$ drives the system from the superradiant phase ($\beta > 1$) where the collective dipole increases with $\tilde{N}$, hence Ω_{Eff} decreases, to the magnetized phase ($\beta < 1$) where $\Omega_{Eff} \approx 0$.

The agreement between the data and the DDM obtained using μ as a single free-parameter is the demonstration that our extended cloud is equivalent to a subwavelength ensemble of $\tilde{N}$ atoms, for which the model is applicable. This striking result, already noticed of the non-driven case [25–27], allows us to investigate the transition between the two non-equilibrium phases predicted by the DDM. To do so we now focus on the steady-state properties of the system.

The steady-state values of the magnetization s_z (APD$\perp$) and emission rate γ_{SR} (APD//) are measured by averaging over a 50 ns-time window before the end of the driving pulse. We report in Fig. 3 (a,b) these values as a function of $\beta = 2\Omega/(\tilde{N}\Gamma)$ for three $\tilde{N}$, together with the theoretical predictions of the DDM. The data, plotted as a function of the scaled parameter β, show both for s_z and γ_{SR} a crossover between two phases. It becomes steeper as $\tilde{N}$ increases and should tend towards a phase transition for $\tilde{N} \to \infty$ [11, 12].

To characterize further the phases, we study the dependence of γ_{SR} with $\tilde{N}$. Fig. 3(c) presents two examples corresponding to different Ω's, together with a polynomial fit $\gamma_{SR} \propto \tilde{N}^{\alpha}$. As reported in Fig. 3(d), the exponent α varies from below 1 in the weak driving regime to 2 in the strong driving one, as was also observed for superradiant lasers [15, 18]. Once again, this is expected from the DDM. For $\beta \gg 1$ (superradiant phase), the populations of Dicke states are saturated and the dipole

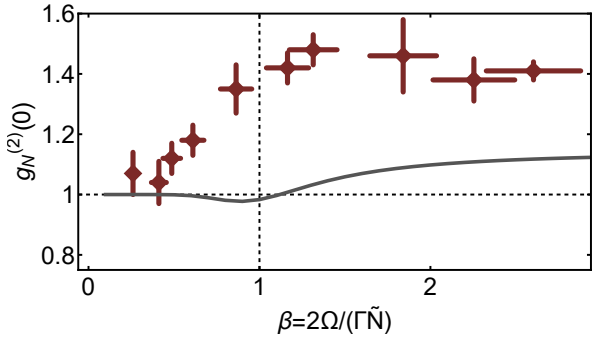

FIG. 4. **Intensity correlations at equal time in the superradiant mode.** Diamonds: $g_N^{(2)}(0)$ as a function of β for $\tilde{N} \simeq 7$. Grey line: theoretical prediction from the DDM for $g_{N,\mathrm{DDM}}^{(2)}(0)$. Error bars: standard deviation of the data evaluated in a window of 5 ns centered around $t = 0$.

vanishes: superradiant spontaneous emission dominates, and $\langle \hat{S}^+\hat{S}^-\rangle \propto \tilde{N}^2$. Conversely, in the magnetized phase ($\beta < 1$) the system develops a collective dipole, and $\gamma_{\mathrm{SR}} = \langle \hat{S}^+\hat{S}^-\rangle \approx |\langle \hat{S}^-\rangle|^2 = \Omega^2/\Gamma^2$, independent of $\tilde{N}$. In the crossover between the two regimes, $\langle \hat{S}^+\hat{S}^-\rangle \sim \tilde{N}$ [22]. The same analysis applied to the numerical solution of the DDM yields results in very good agreement with the data, as shown in Fig. 3(d).

As seen above, the transition separates a phase where a collective dipole is driven by the laser, from a phase where collective spontaneous emission dominates. We therefore expect a change in the statistics of the light emitted by the cloud as we move through the crossover. To explore this, we measure the steady-state intensity correlations at equal times $g_N^{(2)}(0) = \langle (\hat{E}_s^-(t))^2 (\hat{E}_s^+(t))^2\rangle / |\langle \hat{E}_s^-(t)\hat{E}_s^+(t)\rangle|^2$ of the light field $\hat{E}_s$ emitted in the superradiant mode in the far field. To do so we place a 50/50 fibered beamsplitter after the lens collecting this mode, and one APD in each output port [29]. We register the simultaneous coincidences in 1 ns time bins, for the last 50 ns of the laser pulse. Figure 4 presents the measured value of $g_N^{(2)}(0)$ as a function of β. It does show a modification of the statistics of the emitted light around the transition: $g_N^{(2)}(0) \simeq 1$ below threshold ($\beta \leq 1$), indicating that the light has the same statistics than the one of the driving laser field, as expected for a classical dipole in steady-state; in the strong driving regime, $g_N^{(2)}(0)$ saturates around 1.45, thus showing bunching. To compare to the prediction of the DDM, and as $\hat{E}_s^+ \propto \hat{S}^-$ [29], we calculate $g_{N,\mathrm{DDM}}^{(2)}(0) = \langle (\hat{S}^+)^2(\hat{S}^-)^2\rangle / |\langle \hat{S}^+\hat{S}^-\rangle|^2$ [30, 31]. The result is presented in Fig. 4. Despite the lack of quantitative agreement with the experimental data, the DDM also predicts a change in the light statistics at the transition. The quantitative mismatch between the data and the model requires further theoretical investigations. In particular, it may be that despite the good agreement between the DDM and the data observed for the magnetization and γ_{SR}, the model is too simple to calculate the statistical properties of the light emitted by an extended sample, as it ignores the spatial correlations between atoms.

In conclusion, we have realized the DDM in free space and observed the predicted transition between a magnetized and a superradiant non-equilibrium phase. Our observations raise important questions that deserve further investigations. In particular, what is the microscopic justification of the validity of the DDM in free-space for an extended cloud simply using an effective atom number [32, 33]? This works also opens promising prospects for the realization of superradiant laser in free space, e.g. using thermal atomic beams [34]. Finally, increasing the density of the sample could lead to the regime where dipole-dipole interactions between atoms play a role and stabilize exotic non-equilibrium phases [2, 3, 5, 35].

ACKNOWLEDGMENTS

We thank F. Robicheaux for stimulating conversations and A.-M. Rey, J.K. Thompson, K. Moelmer, R.T. Sutherland, J. Marino, D. Dreon and D. Clément for insightful discussions. This project has received funding from the European Research Council (Advanced grant No. 101018511, ATARAXIA) by the Agence National de la Recherche (ANR, project DEAR) and by the Région Ile-de-France in the framework of DIM SIRTEQ (projects DSHAPE and FSTOL).

[1] I. M. Georgescu, S. Ashhab, and F. Nori, Quantum simulation, Rev. Mod. Phys. **86**, 153 (2014).
[2] C. D. Parmee and N. R. Cooper, Phases of driven two-level systems with nonlocal dissipation, Phys. Rev. A **97**, 053616 (2018).
[3] B. Olmos, D. Yu, and I. Lesanovsky, Steady-state properties of a driven atomic ensemble with nonlocal dissipation, Phys. Rev. A **89**, 023616 (2014).
[4] C. D. Parmee and J. Ruostekoski, Signatures of optical phase transitions in superradiant and subradiant atomic arrays, Communications Physics **3**, 205 (2020).
[5] J. A. Muniz, D. Barberena, R. J. Lewis-Swan, D. J. Young, J. R. K. Cline, A. M. Rey, and J. K. Thompson, Exploring dynamical phase transitions with cold atoms in an optical cavity, Nature **580**, 602 (2020).
[6] J. Hannukainen and J. Larson, Dissipation-driven quantum phase transitions and symmetry breaking, Phys. Rev. A **98**, 042113 (2018).
[7] R. H. Dicke, Coherence in spontaneous radiation processes, Phys. Rev. **93**, 99 (1954).
[8] G. S. Agarwal, A. C. Brown, L. M. Narducci, and G. Vetri, Collective atomic effects in resonance fluorescence, Phys. Rev. A **15**, 1613 (1977).
[9] L. M. Narducci, D. H. Feng, R. Gilmore, and G. S. Agarwal, Transient and steady-state behavior of collective atomic systems driven by a classical field, Phys. Rev. A **18**, 1571 (1978).
[10] H. J. Carmichael and D. F. Walls, Hysteresis in the spectrum

for cooperative resonance fluorescence, Journal of Physics B: Atomic and Molecular Physics **10**, L685 (1977).
[11] D. F. Walls, P. D. Drummond, S. S. Hassan, and H. J. Carmichael, Non-Equilibrium Phase Transitions in Cooperative Atomic Systems, Progress of Theoretical Physics Supplement **64**, 307 (1978).
[12] D. F. Walls, Cooperative fluorescence from n coherently driven two-level atoms, Journal of Physics B: Atomic and Molecular Physics **13**, 2001 (1980).
[13] F. Iemini, A. Russomanno, J. Keeling, M. Schirò, M. Dalmonte, and R. Fazio, Boundary time crystals, Phys. Rev. Lett. **121**, 035301 (2018).
[14] D. Meiser, J. Ye, D. R. Carlson, and M. J. Holland, Prospects for a millihertz-linewidth laser, Phys. Rev. Lett. **102**, 163601 (2009).
[15] J. G. Bohnet, Z. Chen, J. M. Weiner, D. Meiser, M. J. Holland, and J. K. Thompson, A steady-state superradiant laser with less than one intracavity photon, Nature **484**, 78 (2012).
[16] M. A. Norcia and J. K. Thompson, Cold-strontium laser in the superradiant crossover regime, Phys. Rev. X **6**, 011025 (2016).
[17] T. Laske, H. Winter, and A. Hemmerich, Pulse delay time statistics in a superradiant laser with calcium atoms, Phys. Rev. Lett. **123**, 103601 (2019).
[18] S. A. Schäffer, M. Tang, M. R. Henriksen, A. A. Jørgensen, B. T. R. Christensen, and J. W. Thomsen, Lasing on a narrow transition in a cold thermal strontium ensemble, Phys. Rev. A **101**, 013819 (2020).
[19] H. Ritsch, P. Domokos, F. Brennecke, and T. Esslinger, Cold atoms in cavity-generated dynamical optical potentials, Rev. Mod. Phys. **85**, 553 (2013).
[20] K. Baumann, C. Guerlin, F. Brennecke, and T. Esslinger, Dicke quantum phase transition with a superfluid gas in an optical cavity, Nature **464**, 1301 (2010).
[21] J. Klinder, H. Keßler, M. R. Bakhtiari, M. Thorwart, and A. Hemmerich, Observation of a superradiant mott insulator in the dicke-hubbard model, Phys. Rev. Lett. **115**, 230403 (2015).
[22] Supplemental material.
[23] A. Glicenstein, G. Ferioli, L. Brossard, Y. R. P. Sortais, D. Barredo, F. Nogrette, I. Ferrier-Barbut, and A. Browaeys, Preparation of one-dimensional chains and dense cold atomic clouds with a high numerical aperture four-lens system, Phys. Rev. A **103**, 043301 (2021).
[24] A. Glicenstein, G. Ferioli, N. Šibalić, L. Brossard, I. Ferrier-Barbut, and A. Browaeys, Collective shift in resonant light scattering by a one-dimensional atomic chain, Phys. Rev. Lett. **124**, 253602 (2020).
[25] M. Gross and S. Haroche, Superradiance: An essay on the theory of collective spontaneous emission, Physics Reports **93**, 301 (1982).
[26] L. Allen and J. H. Eberly, *Optical resonance and two-level atoms* (Dover, 1987).
[27] R. T. Sutherland and F. Robicheaux, Superradiance in inverted multilevel atomic clouds, Phys. Rev. A **95**, 033839 (2017).
[28] G. Ferioli, A. Glicenstein, F. Robicheaux, R. T. Sutherland, A. Browaeys, and I. Ferrier-Barbut, Laser-driven superradiant ensembles of two-level atoms near dicke regime, Phys. Rev. Lett. **127**, 243602 (2021).
[29] R. Loudon, *The quantum theory of light* (OUP Oxford, 2000).
[30] S. Hassan, R. Bullough, R. Puri, and S. Lawande, Intensity fluctuations in a driven dicke model, Physica A: Statistical Mechanics and its Applications **103**, 213 (1980).
[31] H. J. Carmichael, Analytical and numerical results for the steady state in cooperative resonance fluorescence, Journal of Physics B: Atomic and Molecular Physics **13**, 3551 (1980).
[32] K. Debnath, Y. Zhang, and K. Mølmer, Lasing in the superradiant crossover regime, Phys. Rev. A **98**, 063837 (2018).
[33] Y. Zhang, Y.-X. Zhang, and K. Mølmer, Monte-carlo simulations of superradiant lasing, New Journal of Physics **20**, 112001 (2018).
[34] S. B. Jäger, H. Liu, J. Cooper, T. L. Nicholson, and M. J. Holland, Superradiant emission of a thermal atomic beam into an optical cavity, Phys. Rev. A **104**, 033711 (2021).
[35] C. D. Parmee and J. Ruostekoski, Bistable optical transmission through arrays of atoms in free space, Phys. Rev. A **103**, 033706 (2021).
[36] A. Glicenstein, G. Ferioli, A. Browaeys, and I. Ferrier-Barbut, From superradiance to subradiance: exploring the many-body dicke ladder, Opt. Lett. **47**, 1541 (2022).

Supplemental Materials: Observation of a non-equilibrium superradiant phase transition in free space

I. THE DRIVEN-DICKE MODEL

A. Description of the model

The Driven Dicke model considers a system of N-two-level atoms (resonant frequency ω_0), all located at the same position and driven by a laser field with Rabi frequency Ω and detuning Δ with respect to the transition frequency. Since the system size is much smaller than λ, the state evolution is restricted to the $N+1$ permutationally symmetric states containing m excitations [7]. One thus introduces a collective spin operator $\hat{\mathbf{S}} = \sum_{i=1}^{N} \hat{\sigma}_i/2$ (σ_i are the Pauli matrices), and the relevant Hilbert space is spanned by the eigenstates of $\hat{S}_z$, $|S=N/2,m\rangle$, with $-N/2 \leq m \leq N/2$. The actions of the collective spin operators on these states are:

$$\begin{aligned}
\hat{S}^2 |S,m\rangle &= S(S+1)\,|S,m\rangle \\
\hat{S}_z |S,m\rangle &= m\,|S,m\rangle \\
\hat{S}^+ |S,m\rangle &= (\hat{S}_x + i\hat{S}_y)\,|S,m\rangle = A_m\,|S,m+1\rangle \\
\hat{S}^- |S,m\rangle &= (\hat{S}_x - i\hat{S}_y)\,|S,m\rangle = A_{m-1}\,|S,m-1\rangle
\end{aligned} \tag{SM1}$$

where $A_m = \sqrt{S(S+1)-m(m+1)}$. The Hamiltonian describing the interaction of the collective spin with the light is given by

$$\hat{H}_{\mathrm{L}} = \hbar\frac{\Omega}{2}\left(\hat{S}^+ + \hat{S}^-\right) - \hbar\frac{\Delta}{2}\hat{S}_z\,. \tag{SM2}$$

Importantly, the coherent (spin-exchange) component of the dipole-dipole interactions between atoms is ignored in this simplified model: one simply assumes that it leads to a renormalization of the resonant frequency ω_0.

The dynamics of the system is governed by the following master equation:

$$\frac{d\rho}{dt} = -\frac{i}{\hbar}[\hat{H}_{\mathrm{L}},\rho] + \frac{\Gamma}{2}(2\hat{S}^-\rho\hat{S}^+ - \hat{S}^+\hat{S}^-\rho - \rho\hat{S}^+\hat{S}^-)\,. \tag{SM3}$$

In the $|S,m\rangle$ basis, and for the resonant case $\Delta = 0$, it leads to a system of $N(N+1)/2$ coupled differential equations for the matrix elements $\rho_{m,m'} = \langle S,m|\rho|S,m'\rangle$:

$$\begin{aligned}
\dot{\rho}_{m,m'} =& -i\frac{\Omega}{2}(A_{m-1}\rho_{m-1,m'} + A_m\rho_{m+1,m'} \\
&- A_{m'-1}\rho_{m,m'-1} - A_{m'}\rho_{m,m'+1}) \\
&+ \frac{\Gamma}{2}(2A_mA_{m'}\rho_{m+1,m'+1} - A_{m-1}^2\rho_{m,m'} - A_{m'-1}^2\rho_{m,m'})\,.
\end{aligned} \tag{SM4}$$

They can be easily solved numerically for the small atom numbers considered here. From the solutions, we then evaluate the expectation values of the following operators:

$$\begin{aligned}
\langle\hat{S}_z\rangle(t)/N = 2n_e(t) - 1 &= \frac{1}{N}\sum_{m=-S}^{S} m\rho_{m,m}(t) \\
\langle\hat{S}^-\rangle(t) &= \sum_{m=-S}^{S} A_{m-1}\rho_{m,m-1}(t) \\
\langle\hat{S}^+\hat{S}^-\rangle(t) &= \sum_{m=-S}^{S} A_{m-1}^2\rho_{m,m}(t) \\
\langle\hat{S}^+\hat{S}^+\hat{S}^-\hat{S}^-\rangle(t) &= \sum_{m=-S}^{S} A_{m-1}^2A_{m-2}^2\rho_{m,m}(t)\,.
\end{aligned} \tag{SM5}$$

B. Semi-classical approach

The DDM has a semi-classical limit for $N \gg 1$ when considering the average value of the collective spin $\langle\hat{\mathbf{S}}\rangle = (\langle\hat{S}_x\rangle, \langle\hat{S}_y\rangle, \langle\hat{S}_z\rangle)$ [6]. To see it, we use:

$$\frac{d\langle\hat{S}_\alpha\rangle}{dt} = \mathrm{Tr}[\hat{S}_\alpha\frac{d\rho}{dt}] \tag{SM6}$$

combined with the master equation (SM3) and the commutation relations of the spin operators. This leads to the set of coupled, non-linear equations (for $\Delta = 0$):

$$\frac{d\langle\hat{S}_x\rangle}{dt} = \frac{\Gamma}{2}(\langle\hat{S}_x\hat{S}_z\rangle + \langle\hat{S}_z\hat{S}_x\rangle) - \frac{\Gamma}{2}\langle\hat{S}_x\rangle \tag{SM7}$$

$$\frac{d\langle\hat{S}_y\rangle}{dt} = \Omega\langle\hat{S}_z\rangle + \frac{\Gamma}{2}(\langle\hat{S}_y\hat{S}_z\rangle + \langle\hat{S}_z\hat{S}_y\rangle) - \frac{\Gamma}{2}\langle\hat{S}_y\rangle \tag{SM8}$$

$$\frac{d\langle\hat{S}_z\rangle}{dt} = -\Omega\langle\hat{S}_y\rangle - \Gamma(\langle\hat{S}_x^2\rangle + \langle\hat{S}_y^2\rangle)\,. \tag{SM9}$$

We now assume that for large spins (*i.e.* $N \gg 1$), $\langle\hat{S}_\alpha\hat{S}_\beta\rangle \approx \langle\hat{S}_\alpha\rangle\langle\hat{S}_\beta\rangle$ for $\alpha \neq \beta$. Neglecting the dissipative terms $\Gamma\langle\hat{S}_{x,y}\rangle$ of $\mathscr{O}(N)$ only, we then obtain a set of equations that conserves the total spin $\langle\hat{\mathbf{S}}\rangle^2 = \langle\hat{S}_x^2\rangle + \langle\hat{S}_y^2\rangle + \langle\hat{S}_z^2\rangle = N^2/4$. If we now consider that $\langle\hat{S}_x\rangle(0) = 0$, then $\langle\hat{S}^-\rangle(t) = -i\langle\hat{S}_y\rangle$ and the system reduces to two coupled equations:

$$\frac{d\langle\hat{S}^-\rangle}{dt} = \left(i\Omega + \Gamma\langle\hat{S}^-\rangle\right)\langle\hat{S}_z\rangle \tag{SM10}$$

$$\frac{d\langle\hat{S}_z\rangle}{dt} = -i\Omega\langle\hat{S}^-\rangle + \Gamma\left(\frac{N^2}{4} - \langle\hat{S}_z^2\rangle\right)\,. \tag{SM11}$$

The first equation shows explicitly that the dipole $\langle\hat{S}^-\rangle$ is driven by the effective Rabi frequency.

C. Field scattered by the collective dipole inside the cloud

We used in the main text the field radiated inside the cloud by the collective dipole $\langle\hat{E}_{\mathrm{Sc}}\rangle = -i\hbar\Gamma\langle\hat{S}^-\rangle/d$. This expression corresponds to the limit $r \to 0$ (Dicke limit) of the imaginary

part of the field radiated by a dipole $D = d\langle\hat{S}^-\rangle$:

$$E_{\rm Sc} = \frac{D}{4\pi\varepsilon_0}\left[\left(\frac{1}{r^3} - \frac{ik}{r^2}\right)(3\cos^2\theta - 1) + \frac{k^2\sin^2\theta}{r}\right] e^{ikr}, \tag{SM12}$$

using $\hbar\Gamma = d^2k^3/(3\pi\varepsilon_0)$, with $k = \omega_0/c$. The real part of $E_{\rm Sc}$ gives rise to the coherent part of the dipole-dipole interaction. It diverges for $r \to 0$ and is assumed to lead to a renormalization of the resonance frequency ω_0. For the extended sample considered in the experiment, we also neglect the real part of $E_{\rm Sc}$: it would lead to a shift $\Delta\omega$ of the transition frequency in the low excitation intensity limit, and as here the mean interatomic distance fulfills $kr \sim 3$, we expect $\Delta\omega \lesssim \Gamma$. Moreover, for the Rabi frequencies used in the experiment, the shift is suppressed further [24].

II. PREDICTIONS OF THE MODEL

In order to get an intuition about the phases predicted by the DDM, we present here analytical and numerical, steady-state solutions of Eq. (SM4) for the range of parameters Ω/Γ and $\tilde{N}$ accessible in our experiment.

A. Steady-state solution of the semi-classical approach

Equations (SM10) and (SM11) predict that either $\langle\hat{S}^-\rangle = -i\Omega/\Gamma$, in which case $\langle\hat{S}_z\rangle = (N/2)\sqrt{1-\beta^2}$ with $\beta = 2\Omega/(N\Gamma) < 1$, or $\langle\hat{S}_z\rangle = 0$ and $\langle\hat{S}^-\rangle = iN/(2\beta)$, for $\beta > 1$. The value $\beta = 1$ thus appears as a critical point separating two regimes: (i) for $\beta < 1$, the collective spin vector lies on the N-atom Bloch sphere of radius $N/2$, and rotates around the x-axis, from the z-axis to the equatorial plane (y-axis) as β increases up to 1. The angle θ between the spin $\langle\hat{\mathbf{S}}\rangle$ and the z-axis is such that $\tan\theta = |\langle\hat{S}^-\rangle|/|\langle\hat{S}_z\rangle| = \beta/\sqrt{1-\beta^2}$; (ii) when $\beta \geq 1$, the component $\langle\hat{S}_z\rangle$ is locked to 0, while the component $\langle\hat{S}^-\rangle$ along the y-axis decreases as β increases.

B. Numerical solutions of the DDM

Figure SM1 shows the results for the collective dipole $\mathrm{Im}[\langle S^-\rangle]$, the magnetiztion $\langle s_z\rangle$, the effective Rabi frequency $\Omega_{\rm Eff} = \Omega - i\Gamma\langle S^-\rangle$ and the superradiant emission rate $\gamma_{\rm SR}$ as a function of the excitation laser Rabi frequency Ω. We observe two regimes.

In the first one, corresponding to $\Omega/\Gamma \leq N/2$, the collective dipole $\mathrm{Im}[\langle S^-\rangle]$ is proportional to Ω and the screening of the driving field by the field scattered by the collective dipole is efficient. To better understand the screening, we consider the limiting case where $\Omega/\Gamma \ll N/2$. We may then restrict ourselves to the two lowest Dicke states, $|N/2,-N/2\rangle$ and $|N/2,-N/2+1\rangle$, corresponding respectively to $|G\rangle = |ggg...g\rangle$ and $|W\rangle = (|egg...g\rangle + |geg...g\rangle + ...|ggg...e\rangle)/\sqrt{N}$. The matrix element of the collective dipole connecting the two states is $d\sqrt{N}$, with d the single-atom dipole, so that the decay rate of $|W\rangle$ is $N\Gamma$ and the collective coupling to the laser is $\Omega\sqrt{N}$. Restricting ourselves to this two-level system, $\gamma_{SR} = N\Gamma\pi_W$ where $\pi_W \approx (\Omega\sqrt{N})^2/(N\Gamma)^2$ is the population of the $|W\rangle$ state. Hence, $\gamma_{SR} = \Omega^2/\Gamma$, independent of N. Similarly, $\langle S^-\rangle = i\sqrt{N}(\Omega\sqrt{N})/(N\Gamma)$, also independent of N. As we approach $\Omega/\Gamma \lesssim N/2$, however, $\langle S^-\rangle$ remains proportional to Ω despite the fact that we significantly populate the Dicke states up to $m \approx 0$: the suppression of the coherences $\rho_{m,m-1}$ due to the strong driving is counteracted by the enhanced coupling A_{m-1} between Dicke states $|S,m\rangle$ and $|S,m-1\rangle$.

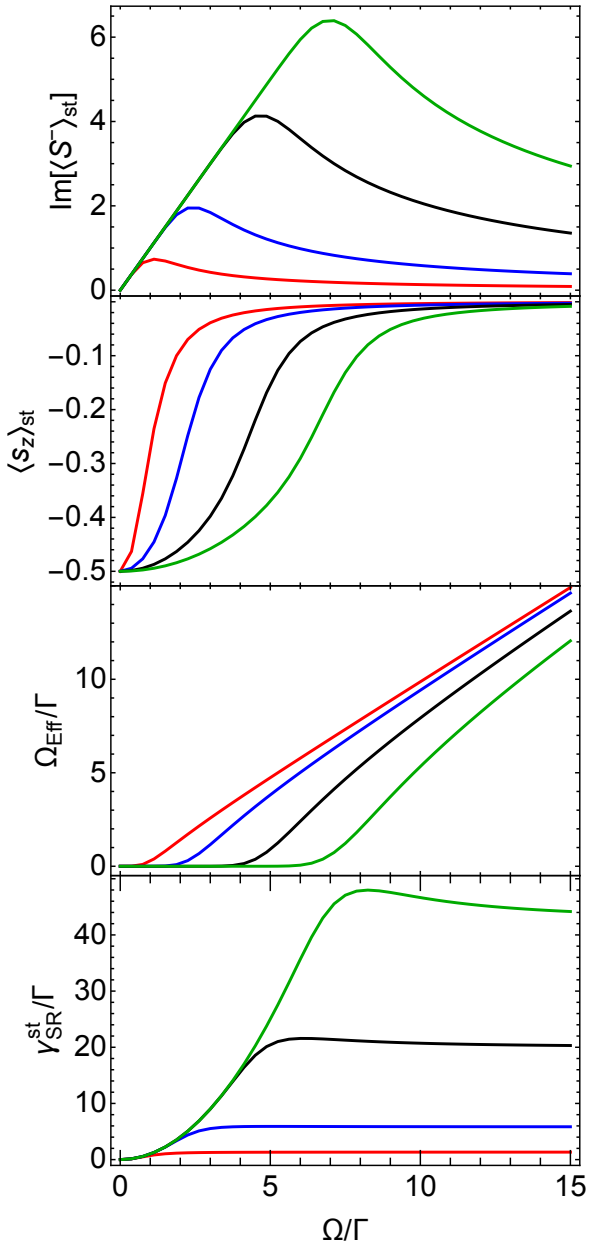

FIG. SM1. **Steady state values** of the collective dipole $\mathrm{Im}[\langle S^-\rangle]$, the magnetiztion $\langle s_z\rangle$, the effective Rabi frequency $\Omega_{\rm Eff}$ and the superradiant emission rate $\gamma_{\rm SR}$ as a function of Ω/Γ, plotted for $N = (2,5,10,15)$ (red, blue, black, green).

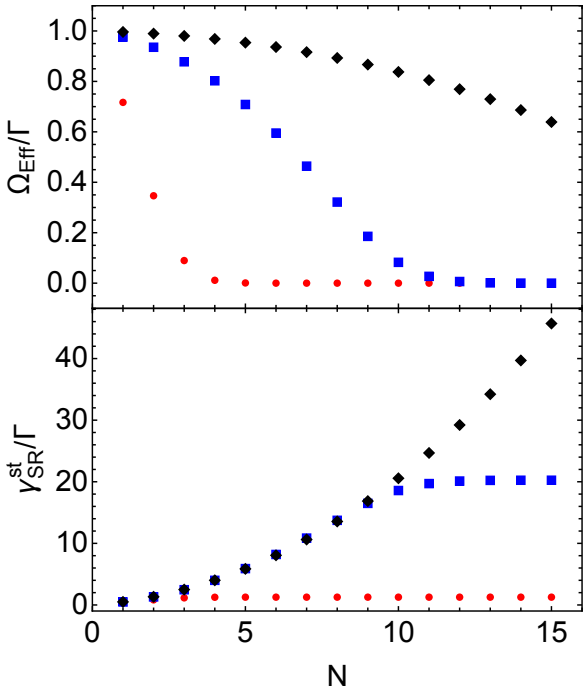

FIG. SM2. **Steady state values** of $\Omega_{\rm Eff}$, and $\gamma_{\rm SR}$ as a function of N, for $\Omega/\Gamma = (1.1, 4.5, 11)$ (red dots, blue squares, black diamonds).

Thus, despite the saturation of the lowest Dicke states, a collective dipole corresponding to a collective Bloch vector can develop even close to the equatorial plan. This would be impossible for a two-level system and this is a feature of the ladder of Dicke states.

In the second regime, $\Omega/\Gamma \gg N/2$, the system is saturated, the collective dipole $\langle S^-\rangle \to 0$, and the population of each Dicke state $|S,m\rangle$ is $\rho_{m,m} = 1/(N+1)$. Calculating the sum in Eqs. (SM5), we get $\gamma_{\rm SR} = N(N+2)/6$, independent of Ω.

We also plot in Fig. SM2 $\Omega_{\rm Eff}$ and $\gamma_{\rm SR}$ as a function of N for different Ω. We confirm that for $N \geq 2\Omega/\Gamma$ the screening from the collective dipole operates, and that $\gamma_{SR} \to \Omega^2/\Gamma$ for $N \to \infty$. We also observe that for increasing values of N starting from 1, $\gamma_{SR} \propto N^\alpha$, with α decreasing from 2 to 0. Such a decrease is observed in the experiment (Fig. 3(c))

C. Analytical derivation of the phase transition

prediction of a second-order phase transition in the thermodynamics limit ($N \to \infty$), following Ref. [12]. The field operator $\hat{E}^+_{\rm Eff}$ inside the cloud is the superposition of the classical laser field $\hat{E}^+_{\rm L}$ and of the fields scattered by all the atoms, $\hat{E}^+_{\rm sc} = -i\hbar\Gamma\hat{S}^-/d$. Hence, $\hat{E}^+_{\rm Eff} = \hat{E}^+_{\rm L} - i\hbar\Gamma\hat{S}^-/d$, leading to

$$\Omega^2 = \frac{\hbar^2}{d^2}\langle \hat{E}^-_{\rm L} E^+_{\rm L}\rangle \approx \Omega^2_{\rm Eff} + \frac{N^2\Gamma^2}{4}\langle \hat{\sigma}^+\hat{\sigma}^-\rangle\,, \qquad \text{(SM13)}$$

with $\hat{S}^- = N\hat{\sigma}^-/2$ and $\Omega^2_{\rm Eff} = \hbar^2\langle \hat{E}^-_{\rm Eff}E^+_{\rm Eff}\rangle/d^2$. We have neglected here the terms $\langle E^-_{\rm Eff}\hat{S}^+\rangle$ and $\langle E^+_{\rm Eff}\hat{S}^-\rangle$, which are of

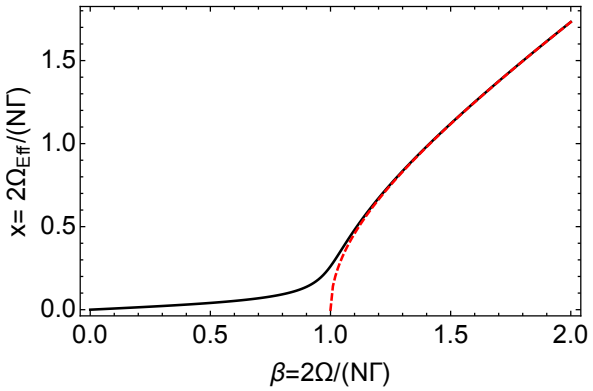

FIG. SM3. **DDM and second order phase transition.** Comparison between the numerical solution of Eq. (SM15) for $N = 20$ (black line), and the analytical solution $x = \sqrt{\beta^2 - 1}$ (red dashed line), showing the existence of a critical point for $N \to \infty$.

order N only. Each two-level atom in the cloud is driven by the effective Rabi frequency $\Omega_{\rm Eff}$, hence:

$$\langle \hat{\sigma}^+\hat{\sigma}^-\rangle = \frac{1}{2}\frac{2\Omega^2_{\rm Eff}/\Gamma^2}{1+2\Omega^2_{\rm Eff}/\Gamma^2} \qquad \text{(SM14)}$$

in steady-state and on resonance ($\Delta = 0$) [26]. Introducing $\beta = 2\Omega/(N\Gamma)$ and $x = 2\Omega_{\rm Eff}/(N\Gamma)$ yields:

$$\beta^2 = x^2 + \frac{N^2x^2/2}{1+N^2x^2/2}\,. \qquad \text{(SM15)}$$

Considering that $N \gg 1$, $x^2 \approx \beta^2 - 1$ for $\beta \geq 1$, hence

$$\beta \geq 1 \Rightarrow x \approx \sqrt{\beta^2 - 1}\,. \qquad \text{(SM16)}$$

For $\beta < 1$, we get $x \ll 1$, so that:

$$\beta^2 \approx \frac{N^2x^2/2}{1+N^2x^2/2} \Rightarrow x \approx \frac{\sqrt{2}}{N}\frac{\beta}{\sqrt{1-\beta^2}}\,. \qquad \text{(SM17)}$$

These two last equations show the existence of a critical point for $\beta = 1$, with $\Omega_{\rm Eff} = 0$ for $\beta < 1$ when $N \to \infty$, reminiscent of a second order phase transition.

It may look inconsistent to obtain $\Omega_{\rm eff} = 0$ while $\langle \hat{S}^-\rangle = -i\Omega/\Gamma \neq 0$ in the case $\beta < 1$, as the effective field is the source of $\hat{S}^-$. However, for large but finite N, $\Omega_{\rm Eff} = \mathcal{O}(1/N)$ [Eq.(SM17)], so that $\langle \hat{S}^-\rangle \propto N\Omega_{\rm Eff}$ remains finite. Figure SM3 shows the numerical solution of Eq. (SM15) for $N = 20$, together with the analytical solution of Eq. (SM16).

III. COOPERATIVE COUPLING BETWEEN AN ATOMIC ENSEMBLE AND A DIFFRACTION MODE

In this section, we evaluate the cooperative coupling between a generic atomic distribution and a diffraction mode in free space. The intensity emitted in a direction **k** by a cloud

containing N atoms is given by [26]:

$$I_N(\mathbf{k}) = I_1(\mathbf{k})\Big[\sum_i^N \frac{\langle\hat{\sigma}_i^z\rangle+1}{2} + \sum_{i\neq j}^N e^{i\mathbf{k}\cdot(\mathbf{r}_i-\mathbf{r}_j)}\langle\hat{\sigma_i^+}\hat{\sigma_j^-}\rangle\Big] \tag{SM18}$$

where $I_1(\mathbf{k})(\langle\hat{\sigma}_i^z\rangle+1)/2$ is the single atom intensity. The first term on the right side of Eq. (SM18) is the *incoherent* intensity emitted by the system. The second term describes the correlations between different atoms and is responsible for the *coherent* part of the emission.

As done in [26] for the non-driven case, we now assume a collective, factorizable atomic state of the N atoms, excited by a laser with a wavevector $\mathbf{k}_\mathrm{L}$: $\langle\hat{\sigma_i^+}\hat{\sigma_j^-}\rangle \approx \langle\hat{\sigma_i^+}\rangle\langle\hat{\sigma_j^-}\rangle = |\langle\hat{\sigma^+}\rangle|^2 e^{-i\mathbf{k}_\mathrm{L}\cdot(\mathbf{r}_i-\mathbf{r}_j)}$. The coherent part of the radiation is then:

$$I_N^{\mathrm{coh}}(\mathbf{k}) = I_1(\mathbf{k})|\langle\hat{\sigma^+}\rangle|^2\sum_{i\neq j}^N e^{i(\mathbf{k}-\mathbf{k}_\mathrm{L})\cdot(\mathbf{r}_i-\mathbf{r}_j)}\ . \tag{SM19}$$

Introducing the structure factor:

$$\Gamma(\mathbf{k},\mathbf{k}_\mathrm{L}) = \frac{1}{N^2}\sum_{i\neq j}^N e^{i(\mathbf{k}-\mathbf{k}_\mathrm{L})(\mathbf{r}_i-\mathbf{r}_j)} \tag{SM20}$$

leads to:

$$I_N^{\mathrm{coh}}(\mathbf{k}) = N^2 I_1(\mathbf{k})|\langle\hat{\sigma^+}\rangle|^2\Gamma(\mathbf{k},\mathbf{k}_\mathrm{L})\ . \tag{SM21}$$

In analogy with cavity QED, we define the cooperative coupling between an extended cloud and a diffraction mode (extending over a solid angle $\Delta\Theta$) as $C_{\mathrm{free}} = P_N^{\mathrm{coh}}/(NP_1)$ where P_N^{coh} is the power radiated by N atoms into the diffraction mode, i.e., $P_N^{\mathrm{coh}} = \int_{4\pi} d\Omega_\mathbf{k} I_N(\mathbf{k})$ and P_1 is the power radiated by a single atom in 4π. In the weak driving regime, $|\langle\hat{\sigma^+}\rangle|^2 \approx (\langle\hat{\sigma}_i^z\rangle+1)/2$ and we get:

$$C_{\mathrm{free}} = \frac{N^2\int_{4\pi} d\Omega_\mathbf{k} I_1(\mathbf{k})\Gamma(\mathbf{k},\mathbf{k}_\mathrm{L})}{N\int_{4\pi} d\Omega_\mathbf{k} I_1(\mathbf{k})} = N\mu\ . \tag{SM22}$$

As the structure factor $\Gamma(\mathbf{k},\mathbf{k}_\mathrm{L})$ has non-zero values only in $\Delta\Theta$, $\mu \sim \Delta\Omega/(4\pi)$. This derivation shows that the cooperativity is nothing but the shape factor introduced in the context of the (non-driven) superradiance in extended clouds [26, 27]. Note that the value of μ depends on the direction of the excitation laser.

We now calculate μ for the specific geometry of our experiment. For circularly polarized dipoles, $I_1(\mathbf{k}) = I_1(\phi,\theta) = (1+\cos^2\phi\sin^2\theta)/2$, with θ and ϕ the polar and azimuthal angles with respect to the quantization axis. ($\hat{k} = (\cos\theta, \sin\theta\cos\phi, \sin\theta\sin\phi)$). Then, $P_1 \propto 8\pi/3$. To calculate $\Gamma(\mathbf{k},\mathbf{k}_\mathrm{L})$ and P_N^{coh}, we replace the sum over discrete positions by an integral over a continuous density distribution $\rho(\mathbf{r})$:

$$\Gamma(\mathbf{k},\mathbf{k}_\mathrm{L}) = \left|\int d^3\mathbf{r}\,\rho(\mathbf{r})\,e^{i\mathbf{r}(\mathbf{k}-\mathbf{k}_\mathrm{L})}\right|^2\ . \tag{SM23}$$

Assuming a Gaussian density $\rho(\mathbf{r})$ with r.m.s. size ℓ_{ax} along $\hat{x}$ and ℓ_{rad} in $\hat{y}$ and $\hat{z}$, setting $\mathbf{k}_\mathrm{L}$ along $\hat{x}$, we obtain:

$$P_N^{\mathrm{coh}} \propto \pi\int_0^\pi d\theta\sin\theta\Big(1+\frac{\sin^2\theta}{2}\Big)\times \exp[-(k\ell_{\mathrm{rad}}\sin\theta)^2]\exp[-(k\ell_{\mathrm{ax}})^2(\cos\theta-1)^2]\ . \tag{SM24}$$

A Taylor expansion of the second exponential in the integral indicates that the integrant is non negligible in the solid angle $\Delta\Theta/(4\pi) \sim \mu \sim \lambda/(2\pi\ell_{\mathrm{ax}})$. With the experimental values ℓ_{ax} and ℓ_{rad}, we get $\mu \simeq 2.5\times10^{-3}$, a factor 2 smaller than the value used in the main text, obtained as a free parameter. However, a precise estimation of the trap size is challenging and subjected to overestimation (due to radiation pressure effects for instance). Considering a 50% error in the measure of ℓ_{ax} makes the result consistent with the value used in the main text.

Finally, we stress that the structure factor, and consequently the value of μ, depends both on the cloud geometry and the direction of the excitation laser $\mathbf{k}_\mathrm{L}$. In previous works [28, 36], we excited the same atomic ensemble, but perpendicularly to the main axis. This led to a value of μ smaller than the one achieved here by one order of magnitude. Consequently, in that case, $\tilde{N} \ll 1$, making it impossible to observe the phase transition.